




Covalent and van der Waals interactions in a vertical heterostructure composed of boron and carbonA. Kochaev ^{1,2,3} K. Katin ^{1,4} M. Maslov ^{1,4} and S. Singh ^{5,*}¹Laboratory of Computational Design of Nanostructures, Nanodevices, and Nanotechnologies, Research Institute for the Development of Scientific and Educational Potential of Youth, Aviatorov street 14/55, Moscow 119620, Russia²Laboratory of Acoustic Microscopy, N. M. Emanuel Science Institute of Biochemical Physics, Russian Academy of Sciences, Kosygina street 4, Moscow 119334, Russia³Research and Education Center “Silicon and Carbon Nanotechnologies,” Ulyanovsk State University, Leo Tolstoy street 42, Ulyanovsk 432017, Russia⁴Department of Condensed Matter Physics, National Research Nuclear University “MEPhI,” Kashirskoe strasse 31, Moscow 115409, Russia⁵Department of Mechanical Engineering, Indian Institute of Technology Indore, Khandwa Road, Simrol, Indore 453552, India

(Received 16 March 2022; revised 7 June 2022; accepted 17 June 2022; published 30 June 2022)

In this paper a covalent assembly of two two-dimensional (2D) materials is investigated. It is shown that borophene with periodic perforation (as one of numerous 2D boron nanoallotropes) and graphenylene can form the vertical heterostructure. This borophene-graphenylene bilayer reduces the dynamic instability inherent in certain types of 2D boron. A detailed study of the nature of the interatomic bonds shows that covalent forces and van der Waals forces act alternately between a pair of neighboring boron and carbon atoms. The electronic and mechanical properties of the predicted heterostructure are comprehensively investigated: in the equilibrium condition, under strain, and with passivation by atomic hydrogen. Several calculation schemes are used to increase the accuracy of the electronic structure calculations. It is shown that the tension and the passivation of borophene-graphenylene from the carbon layer by hydrogen can strongly affect the band gap. The mechanical properties of this heterostructure correspond to the properties of one of its materials, graphenylene. The use of this material to stabilize 2D boron nanoallotropes, as well as in flexural nanoelectronics, is promising.

DOI: [10.1103/PhysRevB.105.235444](https://doi.org/10.1103/PhysRevB.105.235444)**I. INTRODUCTION**

The discovery of graphene [1] spurred the search for new two-dimensional (2D) materials with unique and surprising properties. The synthesis of new materials offers perspectives in the fields of energy, mechanics, electronics, and ecology. As a result of progress made in quantum chemistry over the last decade, the number of new predicted 2D materials has increased significantly. Many of those predicted are soon discovered (synthesized) in chemical laboratories [2]. They include not only 2D materials with a hexagonal lattice such as graphene and its derivatives (graphane, graphdiyne, etc.) but also more curious ones. As rightly noted in Ref. [3], many monolayer materials are geometric prototypes of Kepler nets, and 2D “honeycomb” materials are only one of 11 possible cases. In addition to graphene corresponding to net 6³, 2D materials in the form of *two* nets, 46 12 and 3⁶, are currently being synthesized [4,5].

The former, due to relatively recent discovery [4] but much earlier reference in [6] and subsequent occasional mention, has no well-established name. For example, in a series of papers [7–9] it was known as supracrystal (C)₆₆₄. Scientists who obtained it through dehydration and poly-

merization reactions of 1,3,5-trihydroxybenzene named it 4-6-carbophene [4]. In other works it was called biphenylene carbon [10] and [N]-phenylene [11]. There is also a short name—C64 [12]. Recently, the word “graphenylene” has been used more frequently [13–19], reflecting its affinity to graphene and graphenelike materials. Here we will stick with the latest terminology. Graphenylene is a two-valley direct-gap semiconductor with a narrow band gap, the magnitude of which is easily tuned using the tensile strain or the quantum-size effect when nanoribbons are cut out of it [17,18,20]. It is capable of adsorbing optical photons well and improving photoelectric conversion efficiency [16,19]. The porous morphology of graphenylene also looks promising for sorption and separation of gas particles and ions in solutions.

The second is a no less unique 2D material. It is formed by boron atoms in the states of two- and three-center bonds, which determine its electrodefinite properties and oxidation features in comparison with bulk boron allotropes [21]. Due to the high chemical activity of boron, borophene can have a vast number of low-dimensional allotropes [22–25]. A specific electronic structure, a complex mechanism of the atomic bonding, mechanical properties that are superior to graphene, and significant potential in supercapacitors, batteries, hydrogen storage, and biomedical applications have allowed the authors of the recent review in [26] to call borophene a supermaterial. But because the structural unit of monolayer

*Corresponding author: a.kochaev@gmail.com

borophene materials is a bulk object—the icosahedron B_{12} —their production and further stabilization in the form of single monolayers (in the absence of a substrate) are serious challenges and require innovative approaches.

Currently, borophenes are grown on the following substrates: Au(111) [27], Ag(111) [5,28], Ag(110) [29], Cu(111) [30], Al(111) [31], and Ir(111) [32]. These were used to synthesize β_{12} , χ_3 , χ_6 , striped borophene, and some other types. An alternative to metal substrates could be another idea, namely, the use of other suitable monolayers as a stabilizing agent for the unstable single borophene. Advances in this regard are mainly due to the recent synthesis of borophene-graphene [33] and borophene-borophene vertical heterostructures [34,35], as well as the positive outcomes of theoretical investigations of pure [36] and passivated [37] borophene-graphene bilayers.

As to the above statements, an idea arises: stabilizing borophenes using graphenylene in the form of the vertical assembly formed from two this single layers. Based on previous experience in designing similar heterostructures [36] and the results of experimental works [33,34], here we propose the vertical borophene-graphenylene heterostructure and solve a few problems. First, we offer a way to stabilize monolayer porous striped borophene using graphenylene. Second, we study the chemical nature of the bonds in this assembly. Third, we investigate its electronic and mechanical properties. Finally, we also determine the influence of the passivation by atomic hydrogen on these properties. The proposed items are solved by state-of-the-art methods of quantum chemistry. Since striped borophene and graphene have already been synthesized, the resulting heterostructure corresponds well to the possibilities of modern nanotechnology. The presence of pores makes this material interesting in terms of energy capacity as a material for anodes or cathodes in next-generation batteries. Recently, the potentiality of graphenylene was shown for this purpose [13,38]. In this regard too, some borophenes are very promising [39–41]. At the same time, graphenylene membranes have high permeability and selectivity for certain particles, which makes them an excellent candidate for osmotic applications [42–44]. We believe that the advantages of each of these 2D materials can be successfully used in the stated areas.

II. COMPUTATIONAL METHODS

Our theoretical results are obtained in the framework of density functional theory (DFT) with a linear combination of atomic orbital basis sets and nonequilibrium Green's functions. All calculations, as well as the computational design and visualization, are made using the QUANTUMATK solid-state physics software [45]. The PSEUDODOJO potentials [46] and generalized gradient approximation (GGA) for the exchange and correlation potential expressed by the Perdew-Burke-Ernzerhof (PBE) functional [47] are used in all calculational procedures of optimization. To generate k points in the Brillouin zone, the Monkhorst-Pack method [48] with a $15 \times 15 \times 1$ grid is used. The interaction between the atoms that are not bonded covalently is considered by using the dispersion correction for density functionals (DFT-D3) [49] method of Grimme. All calculations are carried

out using periodic boundary conditions, wherein bilayer slabs are separated from each other by a vacuum region of 20 Å. The structures (under stress and not under stress) are optimized while a Hellman-Feynman force exceeds 3×10^{-3} eV/Å and the convergence threshold between the next two iteration steps becomes less than 10^{-5} . Average C-C and B-B bond lengths obtained from DFT allow us to select potential parameters from different available sets. A comparative molecular dynamics (MD) simulation is based on Tersoff interatomic potentials [50]. To determine the dependence of the electronic properties on the calculation scheme, different exchange-correlation functionals are tested. In addition to GGA with the PBE functional, the Heyd-Scuseria-Ernzerhof (HSE06) hybrid exchange correlation functional [51] is used to correct the band gap values. A $9 \times 9 \times 1$ supercell and a Γ -centered automatic k mesh are chosen to calculate the interatomic forces. The contributions to the dynamical matrix from the DFT-D3 corrections [49] are also fully included in the phonon calculations. The frozen-phonon approach is applied to obtain the phonon spectrum and the phonon density of states. To study the elastic characteristics, we used the finite-displacement method.

III. RESULTS AND DISCUSSION

A. Geometry and bonds characteristic

The vertical heterostructure composed of two known 2D materials was not accidental and was obtained during an optimization procedure of the geometric parameters by minimizing the potential energy function. Initially, a perforation was created in the structure of borophene-graphene. It consisted of the through periodic removal of clusters of boron and carbon atoms in the form of a hexagram (see Fig. 1). At this preoptimization stage, in fact, a computer design of the vertical bilayer heterostructure was performed, consisting of one of the numerous low-dimensional planar boron allotropes and porous graphene [52]. The images of these “parent” materials and their electron and phonon properties are presented in the Supplemental Material [53] separately.

Further, the gradient descent optimization method was applied. When the threshold of all forces acting on the atom was reached (See Sec. II, 3×10^{-3} eV/Å), the heterostructure shown in Fig. 1 was obtained. Graphene was replaced by graphenylene. Let us discuss the result. The transition from porous graphene to graphenylene is due to dangling carbon bonds that have not been passivated. For this reason, in the search for the optimal geometry, bilayer vertical boron-carbon hexagons are rotated towards each other so that instead of one in-plane carbon bond between the carbon hexagons, two are formed at once, as in graphenylene. In this case, there are no dangling carbon bonds, and the system passes into a more stable energy state. According to the names of its parents, the formed vertical heterostructure can be called borophene-graphenylene. Thus, the optimization trajectory reflects the tendency of boron and carbon atoms to lie under each other and form vertical bonds. The vertical covalent bonds are formed only between the boron and carbon atoms of one of the two hexagons in the unit cell, while van der Waals forces act between the atoms of the other (see Fig. 1). The

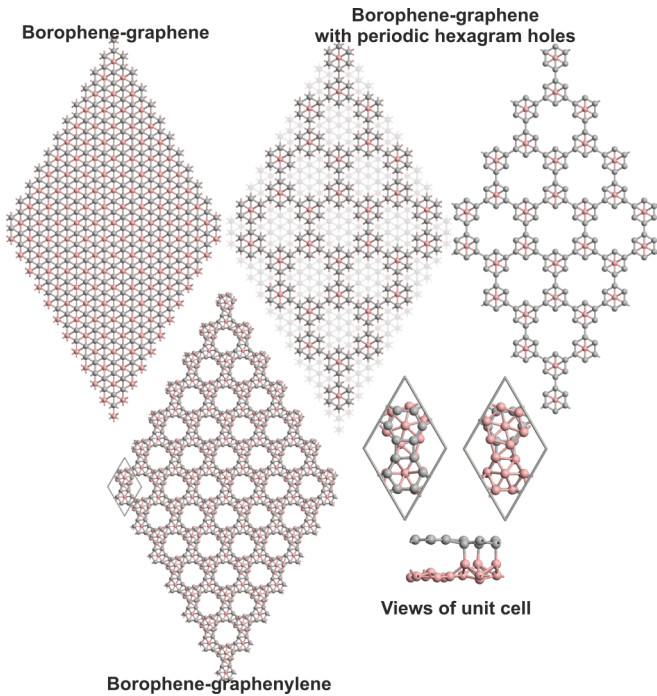


FIG. 1. Schematic representation of the borophene-graphene vertical heterostructure, the borophene-graphene heterostructures with the atomic clusters to be removed (in the form of a hexagram), and the borophene-graphenylene bilayer obtained as a result of solving the optimization problem and the unit cell of this bilayer from different sides.

corresponding conclusion can be illustrated by the calculation of the electron localization function (ELF) of the optimized borophene-graphenylene bilayer.

It is well known [54] that the ELF is defined as

$$\text{ELF} = \frac{1}{1 + (D/D_h)^2}, \quad (1)$$

$$D = \frac{1}{2} \sum_i |\nabla \phi_i|^2 - \frac{1}{8} \frac{|\nabla \rho|^2}{\rho}, \quad (2)$$

$$D_h = \frac{3}{10} (3\pi^2)^{2/3} \rho^{5/3}, \quad (3)$$

where ϕ_i is the Kohn-Sham orbital and ρ is the local density.

Figure 2 shows the calculation results of ELF for borophene-graphenylene.

As pointed out in [54], the ELF, ranging from 0 to 1, takes a value of 0 if there are regions of space where the electrons are perfectly delocalized, and it takes a value of 1 if high electron localization can be observed. When high electron localization is reached between atoms, the bonding is considered covalent and vice versa [37,55]. The isometric surfaces of the ELF depicted in Fig. 2(a) are created for a value of 0.96, reflecting primarily the covalent interaction between atoms. Thus, significant covalent interaction is present where these isosurfaces are found: between all carbon atoms in graphenylene, between three carbon and boron atoms, and also between boron atoms in borophene. As follows from Fig. 2(a), both covalent forces and forces of a smaller order, such as those of a van der Waals nature, act between the layers

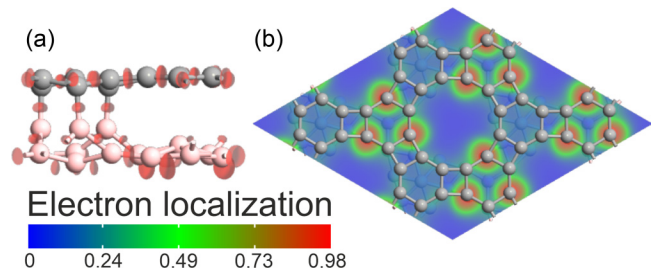


FIG. 2. Electron localization function of the borophene-graphenylene: (a) isometric surface and (b) map. The color bar corresponds to a value of the electron localization function. The interlayer bonds possess the covalent character where the value is high.

of borophene and graphenylene. The map of the ELF [see Fig. 2(b)], projected exactly in the middle between borophene and graphenylene, allows us to establish an interesting feature. The strong covalent and weak van der Waals bonds alternate between a pair of neighboring boron and carbon atoms both within one hexagonal cluster and between clusters within one [6]-phenylene ring. Obviously, this combination of bonds is the most preferable one; therefore, it was obtained during the optimization.

Table I provides an overview of lattice parameters of pure borophene-graphenylene after the optimization compared to graphene, graphenylene, striped borophene, and borophene-graphene. For all materials, the base vector \mathbf{a} is $(1; 0)d$. The base vector \mathbf{b} is $(\frac{1}{2}; \frac{\sqrt{3}}{2})d$ for all materials excepted striped borophene, for which it is $(0; \frac{3+3\sqrt{2}+2\sqrt{3}}{6})d$. The bond lengths for graphenylene, striped borophene, and borophene-graphenylene are averaged.

As shown in the Table I, the carbon skeleton is stretched compared to graphene. This is facilitated by vertical contacts with 2D boron allotropes. The most significant stretching occurs for pure borophene-graphene even though graphene has better elastic characteristics initially. At the same time, the average values of bond lengths between boron atoms in borophene-graphenylene are higher than those values that are inherent in one parent—borophene. This is what made it different from borophene-graphene. The average bond lengths show that the bond tensile is about 3% between boron atoms in the borophene-graphenylene compared to striped borophene. At first glance, the greater stretching of borophene than

TABLE I. The lattice constant d , bond lengths l_{C-C} and l_{B-B} , and interlayer distance z of pure borophene-graphenylene compared to graphene, graphenylene, striped borophene, and borophene-graphene. The values for known materials are provided with references from the literature. All values are in angstroms.

	d	l_{C-C}	l_{B-B}	z_{\min}	z_{\max}
Graphene [56]	2.46	1.42			
Graphenylene [12]	6.76	1.44			
Striped borophene [57]	1.61		1.75		
Borophene-graphene [36]	2.71	1.58	1.74	1.72	2.95
Borophene-graphenylene	6.99	1.50	1.80	1.66	3.12

TABLE II. The average values of the cohesive energies per atom E_{coh} of borophene-graphenylene compared to those of graphene, graphenylene, striped borophene, and borophene-graphene. All values are in eV/atom.

	Graphene	Graphenylene	Striped borophene	Borophene-graphene	Borophene-graphenylene
E_{coh}	7.83	7.40	6.10	6.37	6.27

graphenylene contradicts the idea that striped borophene has the highest elastic characteristics and is weakly deformed in borophene-graphene (0.5% [36]). However, the bilayer structure with perforation (Fig. 1) was chosen as the initial one, which should obviously reduce the elastic energy reserve. The lattice parameter d of borophene-graphenylene is the largest, and it is more loose and porous than the others. The values z_{max} and z_{min} are given to show the spread of interlayer distances between neighboring atoms. An analysis of the bond lengths $l_{\text{C-B}}$ (or z_{min}) makes it possible to estimate the out-of-plane coupling forces between borophene and graphenylene. Obviously, they are higher for borophene-graphenylene than for borophene-graphene. The obtained values of the interlayer distance z_{max} are typical examples of the van der Waals atomic interactions.

B. An estimate of energetic and dynamic stabilities

Cohesion causes the existence of chemical compounds in condensed matter. The cohesive energy (or total binding energy) characterizes the stability of the interacting atomic configuration R_0 with respect to the states of free particles R . It is defined as [58]

$$E_{\text{coh}} = -\left(\frac{E(\{R_0\})}{N} - \frac{E(\{R \rightarrow \infty\})}{N}\right) = \frac{\sum_{i=1}^N E_{\text{free}} - E_{\text{tot}}}{N}, \quad (4)$$

where the energies E_{tot} and E_{free} can be calculated using DFT methods after finding the optimal geometry and are the total energy of the unit cell and the energies of isolated atoms, respectively, and N is the number of atoms in the unit cell.

Obviously, the higher the absolute value of E_{coh} is, the more work must be done to move the atoms to an infinite distance, and the higher the cohesive forces between them are. Since $E_{\text{tot}} < 0$ and $E_{\text{free}} < 0$, E_{coh} is essentially positive. An overview of the graphene cohesion energy is given in Ref. [59], where the theoretical estimates of E_{coh} range from 7.2 to 7.9 eV/atom. The value of graphene cohesion energy obtained in this paper using the proposed methods (see Sec. II) is 7.83 eV/atom.

In Table II, the cohesive energies per atom E_{coh} of borophene-graphenylene compared to graphene, graphenylene, striped borophene, and borophene-graphene are presented. Since they contain different atoms, the average values of the cohesive energies per atom are everywhere assumed.

As shown in Table II, all the presented mono- and bilayers satisfy the energy stability criterion. A maximum of E_{coh} corresponds to graphene; therefore, it is the most stable of the considered materials in the energetic sense. Near

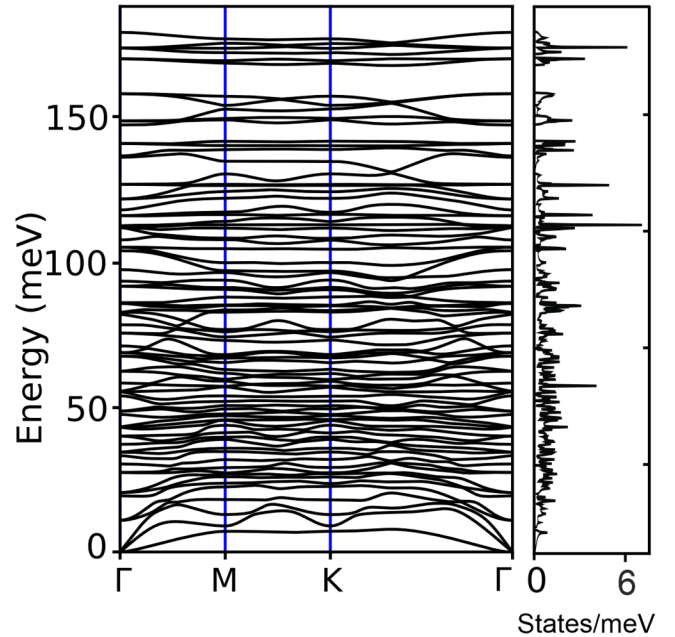


FIG. 3. The phonon spectrum and the phonon density of states of the borophene-graphenylene.

this we find the value of the cohesive energy of graphenylene. The values of E_{coh} of bilayer borophene-graphene and borophene-graphenylene, in turn, are very close to that of striped borophene.

Additionally, the MD simulation of the heterostructure was carried out to determine its stability. After MD optimization, our structure remains a stable, flat bilayer but with small distortions between atoms. The cohesive energy we get equals 5.70 eV/atom at 300 K. The porous structure, which is important for achieving practical goals, remains undistorted.

Since particles of matter are in oscillating motion, the energy criterion is a necessary, but insufficient, condition for the stability of the atomic system. Due to the constant lattice vibrations and no relaxed interatomic bonds, the system can advance to a new configuration state. The study of lattice dynamics allows us to solve the issue and is used as the dynamic stability criterion. We investigated the vibrational properties of borophene-graphenylene for this purpose. Figure 3 shows the phonon spectrum and the phonon density of states along the Γ - M - K - Γ line.

The calculations reveal 3 acoustic and 75 optical branches, corresponding to 26 atoms in the unit cell. The absence of negative branches of acoustic and optical phonons indicates the dynamic stability of a bilayer composed from two 2D materials. A long-wavelength region of the phonon spectrum of well-known monolayer materials (graphene, 2D MoS₂, h -BN, and others) is characterized by a linear dependence of the vibration energy of the in-plane longitudinal-acoustic and transverse-acoustic branches on the wavelength. However, the acoustic out-of-plane (ZA) branch-related vibrations of the atoms in the direction perpendicular to the monolayer display a quadratic dependence. The presented spectrum is characterized by similar behavior, although there is some “hardening” of the ZA mode associated with the existing vertical covalent bonds. As shown in Fig. 3, the extension of acoustic

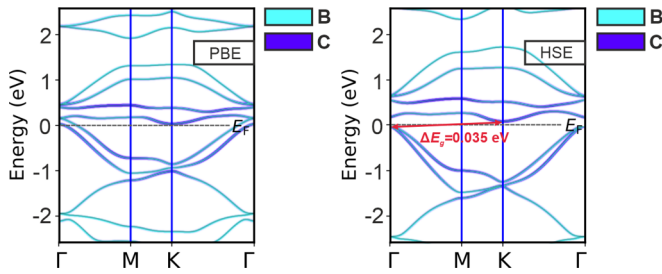


FIG. 4. The electronic band structures of the borophene-graphenylene obtained using the PBE (left) and HSE06 (right) exchange-correlation functionals. The color indicates the contribution of atoms to the corresponding band.

dispersions in the phonon spectrum is less than 20 meV. The total phonon dispersions extend up to 180 meV. The velocity of longitudinal phonons is 14 km/s, and those of planar transverse phonons is 9 km/s [60]. Also a pair of insignificant band gaps ($\Delta E \approx 15$ meV) are found in the phonon spectrum.

So as calculations of the cohesion energy and the phonon spectrum showed, the considered porous borophene-graphenylene material is a stable chemical compound in terms of its energy and dynamic characteristics.

C. Electronic properties

1. Electronic properties upon different functionals

As noted in the Introduction, graphenylene has a narrow band gap. Its value is discussed in Refs. [14,18,61–63] and strongly depends on the calculation scheme used. According to different estimates, the band gap ranges from 0.025 to 1.140 eV. With this in mind, we use two exchange-correlation functionals applied often to 2D materials giving reliable results: PBE and HSE06. Introducing the second functional corrects the underestimation of the semiconductor band gaps, inherent in DFT methods [64]. Figure 4 shows the electronic band structures of borophene-graphenylene obtained using two different calculation schemes.

As follows from Fig. 4, the shapes of the band structures obtained using the different exchange functionals are very similar. However, they have a significant difference. The band overlap established using the PBE functional and determining the absence of the band gap is not found with HSE06. Using HSE06, we found that borophene-graphenylene is an indirect-gap semiconductor with the conduction band minimum (CBM) and the valence band maximum (VBM) located at different points in the Brillouin zone. The band gap ΔE_g is 0.035 eV. We see this result as more plausible because of the known underestimation of the semiconductor band gaps, inherent in DFT [64]. In addition, both graphenylene and porous borophene are semiconductors. The electronic band structures confirming this are presented in the Supplemental Material [53]. The absence of a band gap obtained with PBE and the presence of a band gap obtained with HSE06 have already been encountered for small-gap semiconductors [65,66].

When monolayer materials are assembled into a vertical assembly in the form of multilayer vertical heterostructures, the resulting electronic spectrum should be a superposition

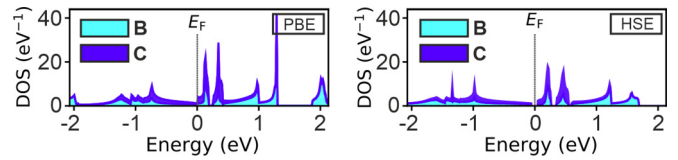


FIG. 5. The projected density of states of the borophene-graphenylene obtained using the PBE (left) and HSE06 (right) exchange-correlation functionals. The color indicates the contribution of atoms to the corresponding states.

of the band structures of individual monolayers with varying degrees of distortion. The stronger the interaction between the layers is, the larger the distortion is. The band structures of van der Waals heterostructures, generally, more accurately repeat the bands of the original materials, which is well illustrated in [67]. For covalent bonded multilayered materials, unlike van der Waals heterostructures, the degree of distortion is maximum. One can see the band structures depicted in Fig. 4 are not an exact repetition or even distorted superposition of the band structures of striped borophene with the periodic hexagram holes and graphenylene (see the Supplemental Material [53]).

The VBM and the CBM are formed by p_z orbitals of boron and carbon atoms with partial mixing of the p_x and p_y orbitals of boron atoms. The p_z orbitals of carbon atoms occupy states mainly in the energy range from -1.5 to 1.5 eV. The s , p_x , p_y , and, with a slight predominance, p_z orbitals of boron atoms dominate in the above energy range. There is strong mixing of the corresponding boron atomic orbitals.

Figure 5 shows the projected density of states of the borophene-graphenylene obtained using two different calculation schemes.

2. Electronic properties upon passivation

Surface passivation is one of three types of doping of 2D materials and heterostructures on their basis. It can significantly change the properties of the passivated material. In the context of this section, we are interested in finding out how passivation by atomic hydrogen affects the electronic properties of borophene-graphenylene. It turns out that striped borophene and graphenylene have completely opposite responses to hydrogen passivation. Although the H functionalization of striped borophene leads to a significant change in the electronic spectrum, the band gap does not open. Due to the high density of itinerant electrons, it is impossible to localize the charge using the hydrogenation of striped borophene [25]. On the contrary, the band gap of graphenylene changes after the H functionalization. It is tuned in a wide range from 0.08 to 4.98 eV due to different degrees of hydrogenation [68].

In Ref. [37] unilateral and bilateral surface passivations of borophene-graphene were considered. It was shown that the hydrogenation of borophene-graphene on the boron side leads to the breaking of chemical bonds between borophene and graphene. Therefore, H passivation on the carbon side of borophene-graphenylene is considered here. We made the high-cost calculations of the electronic band structure of H-passivated borophene-graphenylene using the HSE06

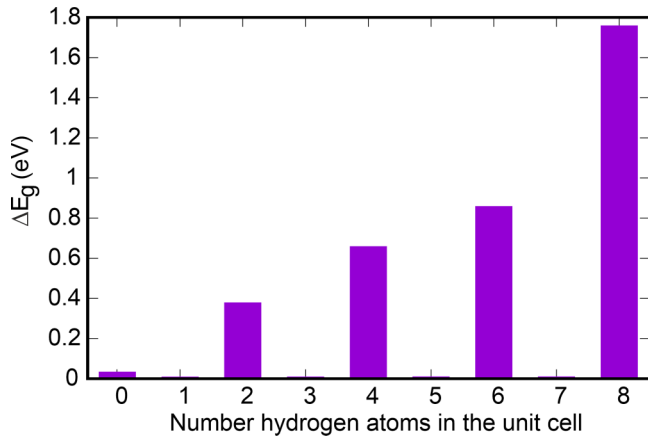


FIG. 6. The dependence of the band gap ΔE_g on the number of hydrogen atoms in the unit cell of borophene-graphenylene.

exchange-correlation scheme. As expected, the covalent bonds between borophene and graphenylene remain intact. Figure 6 shows the calculated values of the band gap depending on the number of hydrogen atoms in the unit cell. The maximum relative concentration of the unilateral passivation is theoretically 0.35 per cell, provided that there are three covalent bonds between carbon and boron atoms in the unit cell. The images of the unit cells, the values of the cohesive energies, and the band gaps of the H-passivated borophene-graphenylene bilayers are presented in the Supplemental Material [53].

The results shown in Fig. 6 demonstrate an interesting feature in the behavior of the electronic properties, namely, odd-even oscillations of ΔE_g with the increase of the hydrogen concentration in the borophene-graphenylene unit cell. An odd number of hydrogen atoms in the unit cell delocalizes the charge, and the band gap disappears ($\Delta E_g = 0$ eV). The fully hydrogenated borophene-graphenylene has no band gap. Given recent advances in controlled sorption [69], this fact may be promising in the area of ultrasensitive sensors and nanoscale separators.

3. Electronic properties upon tension

High tensile strain capacity is another attractive property of 2D materials. Controlled deformations can lead to surprising changes in the electronic properties of 2D materials and van der Waals heterostructures on their basis and to unexpected technological and engineering solutions [70]. The tension of graphene opens the band gap, and the tension of graphenylene increases it [18]. Although the band structure of striped borophene changes significantly under stretching [71], it remains a conductor. As we can see, tensile deformation, like passivation, acts differently on individual borophene and graphenylene monolayers. In this regard, it is interesting to understand how borophene-graphenylene behaves under tension. We considered the tensile deformations before fracture. Figure 7 shows how the initially small band gap of the borophene-graphenylene changes during the biaxial tension.

As follows from Fig. 7, the band gap of borophene-graphenylene increases nonlinearly under biaxial tension.

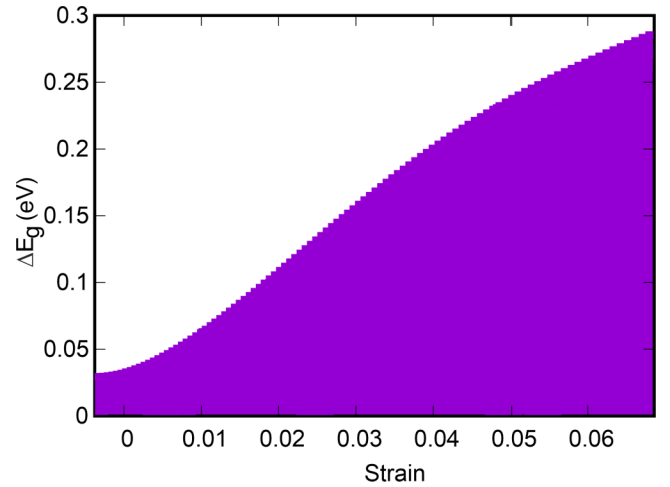


FIG. 7. The dependence of the band gap ΔE_g on the tensile deformation.

Providing a relatively small biaxial tension of 0.06 makes way for increasing the band gap almost 10 times.

So the borophene-graphenylene bilayer can be considered a suitable material for straintronics [70].

D. Elastic properties

1. Initial elastic properties

The elastic response of 2D nanoscale systems should be evaluated by introducing 2D elastic characteristics [72]. Since a physical view of the cross-sectional area on which the deforming tensile (compressive) force acts is undefined for nanoribbons, nanolaces, and other products made from 2D materials, the components of an elastic modulus tensor, like Young's modulus, should be taken in N/m, or, equivalently, in GPa nm [5,73,74]. The relationship between the independent components of the elastic moduli tensor $c_{\alpha\beta}$ and the 2D Young's modulus E_{2D} for two-dimensional hexagonal lattices is given by

$$E_{2D} = \frac{c_{11}^2 - c_{12}^2}{c_{11}}, \quad (5)$$

and the corresponding relationship between them and Poisson's ratio σ is

$$\sigma = \frac{c_{12}}{c_{11}}. \quad (6)$$

Table III lists the calculated components of the elastic modulus tensor in matrix form, the 2D Young's modulus, and Poisson's ratio for borophene-graphenylene compared to hexagonal 2D materials, including graphene, graphenylene, and borophene-graphene. The DFT calculations show that the components of the elastic modulus tensor c_{11} and c_{12} differ by less than 0.5%, and taking into account the hexagonal symmetry of the considered materials, we take $c_{11} \approx c_{22}$.

Striped borophene is not included in Table III since its unit cell is rectangular and, accordingly, the condition of equality of the first two diagonal elements of the matrix of elastic moduli is not satisfied. According to Ref. [57], the elastic properties of striped borophene are characterized by

TABLE III. The components of the elastic modulus tensor in matrix form $c_{\alpha\beta}$ (N/m), the 2D Young's modulus E_{2D} (N/m), and Poisson's ratio σ of borophene-graphenylene compared to mono- and bilayer materials with a hexagonal lattice, including graphene, graphenylene, and borophene-graphene.

	c_{11}	c_{12}	c_{66}	E_{2D}	σ
Graphene [56]	354	60	147	344	0.17
Graphenylene [12]	227	61	83	210	0.27
Borophene-graphene [36]	450	61	194	440	0.14
Borophene-graphenylene	226	39	94	219	0.17

the following constants: $c_{11} = 383$ N/m, $c_{12} = -5.8$ N/m, and $c_{22} = 154$ N/m. The 2D Young's modulus and Poisson's ratio of striped borophene are anisotropic in orthogonal directions: $E_{2D} = 382$ and 154 N/m and $\sigma = -0.04$ and -0.02 . The data presented in Table III suggest that the equilibrium elastic properties of borophene-graphenylene are closest to graphenylene. Its 2D Young's modulus is inferior to that of graphene and, moreover, to that of borophene-graphene. This is obviously due to the porous structure. However, Poisson's ratio for borophene-graphenylene indicates that the plasticity properties are similar to those of graphene [75].

Next, we explore the effect of hydrogenation.

2. Elastic properties upon passivation

As a rule, surface passivation of 2D materials should lead to a deterioration in the elastic response, in particular, a decrease in the 2D Young's modulus. But there are the other consequences too. Passivated graphene (graphane) does, in fact, worsen the elastic response. But what is far more interesting is the C and W configurations of graphane have a very small Poisson's ratio, and B-graphane, in general, is characterized by axial-auxetic behavior [56]. Striped borophane has anisotropic mechanical properties, just like pure striped borophene. H passivation of borophene reduces the ratios of the 2D Young's moduli in the orthogonal directions from 2.33 for borophene to 1.56 for borophane [76].

The calculation results for the elastic characteristics of borophene-graphenylene passivated on the carbon side by atomic hydrogen are presented below. They correspond to two types of H passivation that do not lead to distortion of the atomic configuration of borophene-graphenylene. The first is partially H passivated borophene-graphenylene with three hydrogen atoms per unit cell (see the Supplemental Material [53]). It has the following elastic characteristics: $c_{11} =$

182 N/m, $c_{12} = 25$ N/m, $E_{2D} = 179$ N/m, and $\sigma = 0.14$. The second is borophene-graphenylene completely passivated on the carbon side (see the Supplemental Material [53]). Its elastic characteristics are $c_{11} = 172$ N/m, $c_{12} = 29$ N/m, $E_{2D} = 167$ N/m, and $\sigma = 0.17$. As can be seen from the presented data, the 2D Young's modulus does decrease when the passivation increases. An increase in the number of adsorbed particles on the surface of the vertical heterostructure reduces the overall elasticity due to a smaller weakening of the transverse forces where carbon atoms remain "sandwiched" between boron and hydrogen. At the same time, as follows from the values of c_{12} , the elasticity under shear deformations increases, which leads to an increase in Poisson's ratio.

IV. CONCLUSIONS

Due to its high reactivity, boron combines well with carbon in the 2D form. Striped borophene with periodic perforation in the form of hexagram holes creates a dynamically and energetically stable vertical heterostructure with graphenylene. It is distinguished by interlayer alternating covalent and van der Waals bonds and has a porous structure. This bilayer can serve to improve the stability of 2D boron nanoallotropes, which are known to be prone to dynamic instability. For this heterostructure, the quadratic dependence (like for monolayers) of the energy ZA phonons on the wave vector is satisfied. Using HSE06, borophene-graphenylene is found to be an indirect narrow-gap semiconductor. Its band gap can be tuned by the hydrogenation and the tension. The studied properties and the calculated characteristics are very useful for the design of new devices based on the *covalent* bonding of 2D materials.

On the issue of obtaining the bilayer, we hope that it can be formed by one of the modern methods for obtaining *atomic-sized* pores. This theoretical study will encourage researchers to create pores in borophene-graphene [33] and borophene-borophene [34] vertical heterostructures using particle irradiation or ball milling and ultrasonic processes [77], which, we believe, will also make it possible to detect new porous heterostructures, including borophene-graphenylene.

ACKNOWLEDGMENTS

The presented study was performed with the financial support of the Russian Science Foundation (Grant No. 21-73-00009). A.K. is extremely grateful to DSEPY-RY for the provided computing resources as well as comprehensive support of the presented study.

-
- [1] K. S. Novoselov, D. Jiang, F. Schedin, T. J. Booth, V. V. Khotkevich, S. V. Morozov, and A. K. Geim, *Proc. Natl. Acad. Sci. USA* **102**, 10451 (2005).
- [2] S. Alam, M. A. Chowdhury, A. Shahid, R. Alam, and A. Rahim, *FlatChem* **30**, 100305 (2021).
- [3] A. I. Kochaev, *AIP Adv.* **7**, 025202 (2017).
- [4] Q.-S. Du, P.-D. Tang, H.-L. Huang, F.-L. Du, K. Huang, N.-Z. Xie, S.-Y. Long, Y.-M. Li, J.-S. Qiu, and R.-B. Huang, *Sci. Rep.* **7**, 40796 (2017).
- [5] A. J. Mannix, X.-F. Zhou, B. Kiraly, J. D. Wood, D. Alducin, B. D. Myers, X. Liu, B. L. Fisher, U. Santiago, J. R. Guest, M. J. Yacaman, A. Ponce, A. R. Oganov, M. C. Hersam, and N. P. Guisinger, *Science* **350**, 1513 (2015).
- [6] A. T. Balaban, C. C. Rentea, and E. Ciupitu, *Rev. Roum. Chim.* **13**, 231 (1968) [Erratum, *ibid.*, p. 1233].
- [7] R. A. Brazhe, A. I. Kochaev, and V. S. Nefedov, *Phys. Solid State* **54**, 1430 (2012).

- [8] R. A. Brazhe, A. I. Kochaev, and A. A. Sovetkin, *Phys. Solid State* **55**, 2094 (2013).
- [9] R. A. Brazhe, A. I. Kochaev, and A. A. Sovetkin, *Phys. Solid State* **55**, 1925 (2013).
- [10] R. H. Baughman, H. Eckhardt, and M. Kertesz, *J. Chem. Phys.* **87**, 6687 (1987).
- [11] J. M. Schulman and R. L. Disch, *J. Phys. Chem. A* **111**, 10010 (2007).
- [12] H. Sun, S. Mukherjee, M. Daly, A. Krishnan, M. H. Karigerasi, and C. V. Singh, *Carbon* **110**, 443 (2016).
- [13] Y.-X. Yu, *J. Mater. Chem. A* **1**, 13559 (2013).
- [14] Q. Song, B. Wang, K. Deng, X. Feng, M. Wagner, J. D. Gale, K. Müllen, and L. Zhi, *J. Mater. Chem. C* **1**, 38 (2013).
- [15] S. Rouhi and A. Ghasemi, *Mater. Res.* **20**, 1 (2016).
- [16] L. Zhu, Y. Jin, Q. Xue, X. Li, H. Zheng, T. Wu, and C. Ling, *J. Mater. Chem. A* **4**, 15015 (2016).
- [17] G. S. Fabris, C. E. Junkermeier, and R. Paupitz, *Comput. Mater. Sci.* **140**, 344 (2017).
- [18] R. M. Meftakhutdinov, R. T. Sibatov, and A. I. Kochaev, *J. Phys.: Condens. Matter* **32**, 345301 (2020).
- [19] M. S. Motallebipour and J. Karimi-Sabet, *Phys. Chem. Chem. Phys.* **23**, 14706 (2021).
- [20] E. Perim, R. Paupitz, P. A. S. Autreto, and D. S. Galvao, *J. Phys. Chem. C* **118**, 23670 (2014).
- [21] A. A. Kistanov, S. K. Khadiullin, S. V. Dmitriev, and E. A. Korznikova, *Chem. Phys. Lett.* **728**, 53 (2019).
- [22] H. Tang and S. Ismail-Beigi, *Phys. Rev. Lett.* **99**, 115501 (2007).
- [23] E. S. Penev, S. Bhowmick, A. Sadrzadeh, and B. I. Yakobson, *Nano Lett.* **12**, 2441 (2012).
- [24] X. Wu, J. Dai, Y. Zhao, Z. Zhuo, J. Yang, and X. C. Zeng, *ACS Nano* **6**, 7443 (2012).
- [25] A. A. Kistanov, Y. Cai, K. Zhou, N. Srikanth, S. V. Dmitriev, and Y.-W. Zhang, *Nanoscale* **10**, 1403 (2018).
- [26] M. Ou, X. Wang, L. Yu, C. Liu, W. Tao, X. Ji, and L. Mei, *Adv. Sci.* **8**, 2001801 (2021).
- [27] B. Kiraly, X. Liu, L. Wang, Z. Zhang, A. J. Mannix, B. L. Fisher, B. I. Yakobson, M. C. Hersam, and N. P. Guisinger, *ACS Nano* **13**, 3816 (2019).
- [28] B. Feng, J. Zhang, Q. Zhong, W. Li, S. Li, H. Li, P. Cheng, S. Meng, L. Chen, and K. Wu, *Nat. Chem.* **8**, 563 (2016).
- [29] Q. Zhong, L. Kong, J. Gou, W. Li, S. Sheng, S. Yang, P. Cheng, H. Li, K. Wu, and L. Chen, *Phys. Rev. Materials* **1**, 021001(R) (2017).
- [30] H. Liu, J. Gao, and J. Zhao, *Sci. Rep.* **3**, 3238 (2013).
- [31] W. Li, L. Kong, C. Chen, J. Gou, S. Sheng, W. Zhang, H. Li, L. Chen, P. Cheng, and K. Wu, *Sci. Bull.* **63**, 282 (2018).
- [32] N. A. Vinogradov, A. Lyalin, T. Taketsugu, A. S. Vinogradov, and A. Preobrajenski, *ACS Nano* **13**, 14511 (2019).
- [33] X. Liu and M. C. Hersam, *Sci. Adv.* **5**, eaax6444 (2019).
- [34] X. Liu, Q. Li, Q. Ruan, M. S. Rahn, B. I. Yakobson, and M. C. Hersam, *Nat. Mater.* **21**, 35 (2021).
- [35] C. Chen, H. Lv, P. Zhang, Z. Zhuo, Y. Wang, C. Ma, W. Li, X. Wang, B. Feng, P. Cheng, X. Wu, K. Wu, and L. Chen, *Nat. Chem.* **14**, 25 (2021).
- [36] A. Kochaev, K. Katin, M. Maslov, and R. Meftakhutdinov, *J. Phys. Chem. Lett.* **11**, 5668 (2020).
- [37] A. Kochaev, R. Meftakhutdinov, R. Sibatov, K. Katin, M. Maslov, and V. Efimov, *Appl. Surf. Sci.* **562**, 150150 (2021).
- [38] C. Xu and X. Luo, *ACS Appl. Energy Mater.* **5**, 4970 (2022).
- [39] Y. Zhang, Z.-F. Wu, P.-F. Gao, S.-L. Zhang, and Y.-H. Wen, *ACS Appl. Mater. Interfaces* **8**, 22175 (2016).
- [40] S. Leng, X. Sun, Y. Yang, and R. Zhang, *Mater. Res. Express* **6**, 085504 (2019).
- [41] J. Li, G. A. Tritsarlis, X. Zhang, B. Shi, C. Yang, S. Liu, J. Yang, L. Xu, J. Yang, F. Pan, E. Kaxiras, and J. Lu, *J. Electrochem. Soc.* **167**, 090527 (2020).
- [42] R. I. Babicheva, M. Dahanayaka, B. Liu, E. A. Korznikova, S. V. Dmitriev, M. S. Wu, and K. Zhou, *Mater. Sci. Eng.: B* **259**, 114569 (2020).
- [43] L. Zhu, Q. Xue, X. Li, Y. Jin, H. Zheng, T. Wu, and Q. Guo, *ACS Appl. Mater. Interfaces* **7**, 28502 (2015).
- [44] J. Xu, S. Zhou, P. Sang, J. Li, and L. Zhao, *J. Mater. Sci.* **52**, 10285 (2017).
- [45] S. Smidstrup *et al.*, *J. Phys.: Condens. Matter* **32**, 015901 (2019).
- [46] M. van Setten, M. Giantomassi, E. Bousquet, M. Verstraete, D. Hamann, X. Gonze, and G.-M. Rignanese, *Comput. Phys. Commun.* **226**, 39 (2018).
- [47] J. P. Perdew, K. Burke, and M. Ernzerhof, *Phys. Rev. Lett.* **77**, 3865 (1996).
- [48] H. J. Monkhorst and J. D. Pack, *Phys. Rev. B* **13**, 5188 (1976).
- [49] S. Grimme, J. Antony, S. Ehrlich, and H. Krieg, *J. Chem. Phys.* **132**, 154104 (2010).
- [50] J. Tersoff, *Phys. Rev. B* **39**, 5566 (1989).
- [51] J. Heyd, G. E. Scuseria, and M. Ernzerhof, *J. Chem. Phys.* **118**, 8207 (2003).
- [52] P. Xu, J. Yang, K. Wang, Z. Zhou, and P. Shen, *Chin. Sci. Bull.* **57**, 2948 (2012).
- [53] See Supplemental Materials at <http://link.aps.org/supplemental/10.1103/PhysRevB.105.235444> for the electron and phonon properties of borophene and graphenylene and the cohesive energies and the band gaps of H-passivated borophene-graphenylene.
- [54] B. Silvi and A. Savin, *Nature (London)* **371**, 683 (1994).
- [55] Y. Yin, D. Li, Y. Hu, G. Ding, H. Zhou, and G. Zhang, *Nanotechnology* **31**, 315709 (2020).
- [56] E. Cadelano, P. L. Palla, S. Giordano, and L. Colombo, *Phys. Rev. B* **82**, 235414 (2010).
- [57] B. Peng, H. Zhang, H. Shao, Z. Ning, Y. Xu, G. Ni, H. Lu, D. W. Zhang, and H. Zhu, *Mater. Res. Lett.* **5**, 399 (2017).
- [58] A. Yakoubi, O. Baraka, and B. Bouhafis, *Results Phys.* **2**, 58 (2012).
- [59] V. V. Ivanovskaya, A. Zobelli, D. Teillet-Billy, N. Rougeau, V. Sidis, and P. R. Briddon, *Eur. Phys. J. B* **76**, 481 (2010).
- [60] A. I. Kochaev and R. A. Brazhe, *Acta Mech.* **222**, 193 (2011).
- [61] G. Brunetto, P. A. S. Autreto, L. D. Machado, B. I. Santos, R. P. B. dos Santos, and D. S. Galvao, *J. Phys. Chem. C* **116**, 12810 (2012).
- [62] A. N. Enyashin and A. L. Ivanovskii, *Phys. Status Solidi B* **248**, 1879 (2011).
- [63] R. A. Brazhe and R. M. Meftakhutdinov, *Tech. Phys.* **61**, 750 (2016).
- [64] C. Xia, J. Du, X. Huang, W. Xiao, W. Xiong, T. Wang, Z. Wei, Y. Jia, J. Shi, and J. Li, *Phys. Rev. B* **97**, 115416 (2018).
- [65] J. A. Kurzman, M.-S. Miao, and R. Seshadri, *J. Phys.: Condens. Matter* **23**, 465501 (2011).

- [66] Z. Zhu, B. Dong, H. Guo, T. Yang, and Z. Zhang, *Chin. Phys. B* **29**, 046101 (2020).
- [67] R. M. Meftakhutdinov, R. T. Sibatov, A. I. Kochaev, and D. A. Evseev, *Phys. Chem. Chem. Phys.* **23**, 14315 (2021).
- [68] W. Liu, M. Miao, and J. Liu, *RSC Adv.* **5**, 70766 (2015).
- [69] J. H. Jørgensen, A. G. Čabo, R. Balog, L. Kyhl, M. N. Groves, A. M. Cassidy, A. Bruix, M. Bianchi, M. Dendzik, M. A. Arman, L. Lammich, J. I. Pascual, J. Knudsen, B. Hammer, P. Hofmann, and L. Hornekaer, *ACS Nano* **10**, 10798 (2016).
- [70] I. V. Antonova, *Phys. Usp.* **65**(6) (2022).
- [71] X. Wang, R. Wu, T. Xu, and Y. Gao, *Mater. Res. Express* **8**, 065003 (2021).
- [72] R. C. Andrew, R. E. Mapasha, A. M. Ukpong, and N. Chetty, *Phys. Rev. B* **85**, 125428 (2012).
- [73] J. Yuan, N. Yu, K. Xue, and X. Miao, *RSC Adv.* **7**, 8654 (2017).
- [74] B. Mortazavi, O. Rahaman, M. Makaremi, A. Dianat, G. Cuniberti, and T. Rabczuk, *Physica E (Amsterdam, Neth.)* **87**, 228 (2017).
- [75] J. Haines, J. Léger, and G. Bocquillon, *Annu. Rev. Mater. Res.* **31**, 1 (2001).
- [76] Z. Wang, T.-Y. Lü, H.-Q. Wang, Y. P. Feng, and J.-C. Zheng, *Phys. Chem. Chem. Phys.* **18**, 31424 (2016).
- [77] Y. Li, K. Yin, L. Wang, X. Lu, Y. Zhang, Y. Liu, D. Yan, Y. Song, and S. Luo, *Appl. Catal., B* **239**, 537 (2018).